

An assessment of high-power light-emitting diodes for high frame rate schlieren imaging

Christian E. Willert · Daniel M. Mitchell ·
Julio Soria

Received: 23 February 2011 / Revised: 2 March 2012 / Accepted: 20 March 2012 / Published online: 5 April 2012
© Springer-Verlag 2012

Abstract The feasibility of using high-power light-emitting diodes (LED) as a light source for high frame rate schlieren imaging is investigated. Continuous sequences of high-intensity light pulses are achieved by overdriving the LED with current pulses up to a factor of ten beyond its specifications. In comparison to commonly used pulsed light sources such as gas discharge lamps and pulsed lasers, the pulsed LED has several attractive advantages: the pulse-to-pulse intensity variation is on the same order of magnitude as the detector (camera) noise permitting quantitative intensity measurements. The LED's narrow emission bandwidth reduces chromatic aberrations, yet it is spectrally wide enough to prevent the appearance of speckle and diffraction effects in the images. Most importantly, the essentially lag-free light emission within tens of nanoseconds of the applied current pulse allows the LED to be operated at varying frequencies (i.e., asynchronously), which generally is not possible with neither lasers nor discharge lamps. The pulsed LED source, driven by a simple driver circuit, is demonstrated on two schlieren imaging setups. The first configuration visualizes the temporal evolution of shock structures and sound waves of

an under-expanded jet that is impinging on a rigid surface at frame rates of 500 kHz to 1 MHz. In a second application, long sequences of several thousand high-resolution images are acquired on a free jet at a frame rate of 1 kHz. The low-intensity fluctuation and large sample number allow a reliable computation of two-point correlation data from the image sequences.

1 Introduction

Recent advances in light-emitting diode (LED) technology have resulted in high-power, single-chip devices with luminous radiant fluxes exceeding several watts. When operated with short-duration high-current pulses that significantly exceed the rated currents, the instantaneous light emission of an LED can be increased significantly (Stasicki et al. 1984). As shown by Hiller et al. (1987), the emitted light was, in principle, capable of acquiring Mach–Zehnder interferograms at frame rates in the MHz range. In their application, a single LED was coupled into a monofiber and pulsed with currents of up to 10 A at a frequency of 10 kHz. The principle was later used by Bretthauer et al. (1991) to provide pulsed illumination for a high-speed multiple-image camera based on the Cranz–Schardin principle. The optical arrangement imaged eight separate fiber-coupled LEDs sequentially onto eight separated CCD sensors via an eight-faceted mirror pyramid. This setup permitted image frame rates of up to 10 MHz with the LEDs being pulsed at similar durations (50 ns ... 1 μ s). More recently, the Cranz–Schardin imaging principle has been demonstrated in a configuration that uses a single CCD sensor to image the light of several pulsed LEDs onto separate areas allowing even higher frame rates (Buttsworth 2008; Deblock et al. 2007).

C. E. Willert (✉)
DLR Institute of Propulsion Technology,
German Aerospace Center, 51170 Köln, Germany
e-mail: chris.willert@dlr.de

D. M. Mitchell · J. Soria
Laboratory for Turbulence Research in Aerospace
and Combustion (LTRAC), Department of Mechanical
and Aerospace Engineering, Monash University,
Melbourne, VIC 3800, Australia

J. Soria
Department of Aeronautical Engineering,
King Abdulaziz University, Jeddah, Kingdom of Saudi Arabia

In an extension to the work by Stasicki et al. (1984, 1990), the principle of pulsed light emission from overdriven LEDs was recently investigated by Willert et al. (2010) for modern high-power LED devices on the background of possible application to particle-based flow velocimetry. The investigated devices are designed to operate at continuous currents of up to 18 A and can be operated reliably with pulsed currents exceeding 200 A with which the momentary luminous flux can be increased by a factor of 5–8. The intensity levels provided by the overdriven LEDs are comparable to the intensity of photographic (xenon) flash units and therefore have potential as suitable light sources for schlieren imaging. Compared to the commonly used xenon flash units, an LED essentially instantly responds to current pulses with rise times on the order of 100 ns, thereby enabling stroboscopic illumination at megahertz rates. As will be documented later, the LED provides very repeatable illumination intensities in comparison to a xenon light flash lamp. Further, the broader emission spectrum of an LED with respect to a laser avoids the generation of light speckle on the image sensor, which often arise due to the presence of diffracting elements along the optical path, such as the knife edge in a schlieren setup.

The following article summarizes efforts of using a high-power LED operated in pulsed mode as a light source for schlieren imaging purposes. Different from previous work is that a single LED is pulsed with high currents at much higher repetition rates than reported for instance in (Willert et al. 2010). The first part of the paper provides some background information on the pulsed operation of high-power LEDs. The second part is dedicated to two exemplary applications of the pulsed LED source in schlieren imaging of a supersonic under-expanded free jet.

2 Pulsed LED operation at high repetition rates

Following earlier investigations by Willert et al. (2010), the pulsed operation of high-power LEDs is extended to frequencies up to the MHz range. The utilized self-made driver circuit is described with more detail in (Willert et al. 2010) and presented in Fig. 1 in a simplified form. The circuit's operation is fairly straightforward: capacitor **C1** is first charged to a voltage V_s after which the transistor **T1** is switched on via the driver unit **U1**. This discharges the capacitor to ground with the current I_f flowing through the LED **LD1** causing it to emit light. By measuring the voltage drop across the small resistance **R2** ($0.02\ \Omega$) between the transistor source and ground, the current I_f flowing through the LED can be calculated.

Driving the LED with excessive currents, even for short durations, will lead to thermal damage and subsequent

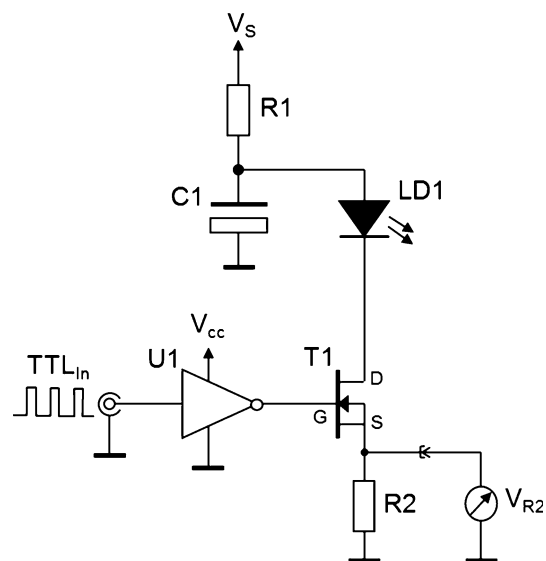


Fig. 1 Simplified version of the LED driver circuit

failure of the device. This was investigated systematically in (Willert et al. 2010) by gradually raising the pulse current for a given pulse width until failure occurred. In particular, it was found that the current levels could be increased with decreasing pulse durations. However, these data were obtained at rather low frequencies around 25 Hz with a correspondingly low duty cycle. For the present application, however, the duty cycle is increased up to 50 %, while the diode is operated in burst mode (here around 100 pulses). The current-pulse damage thresholds determined in (Willert et al. 2010), therefore, do not apply here and require a trial-and-error approach in obtaining reliable current levels.

2.1 Short pulse response characteristics

The response of the LED to short current pulses, in particular, its time-dependent electroluminescence (light emission), was further investigated using a fast laser diode driver (LDP-V 50-100 V3, PicoLAS GmbH) that is specifically designed to have both fast rise and decay times. The LED [Luminus, Phlatlight CBT-120, green (Luminus 2008)] was subjected to $f = 1\ \text{kHz}$ current pulses of $I_f = 50\ \text{A}$ and 250 ns duration. The observed decay times in the photodiode signal (Fig. 2, top) are similar to those produced by the self-designed pulsed current source mentioned before. The observed electroluminescence decay time of about 350 ns results from the recombination of remaining charge carriers in the LED after the end of the pulse. This decay time depends on the type of LED as illustrated in Fig. 2, bottom, for a smaller LED device (LXHL-PM02, green, Philips Lumileds). For this device, the decay time reduces down to about 150 ns. The decay

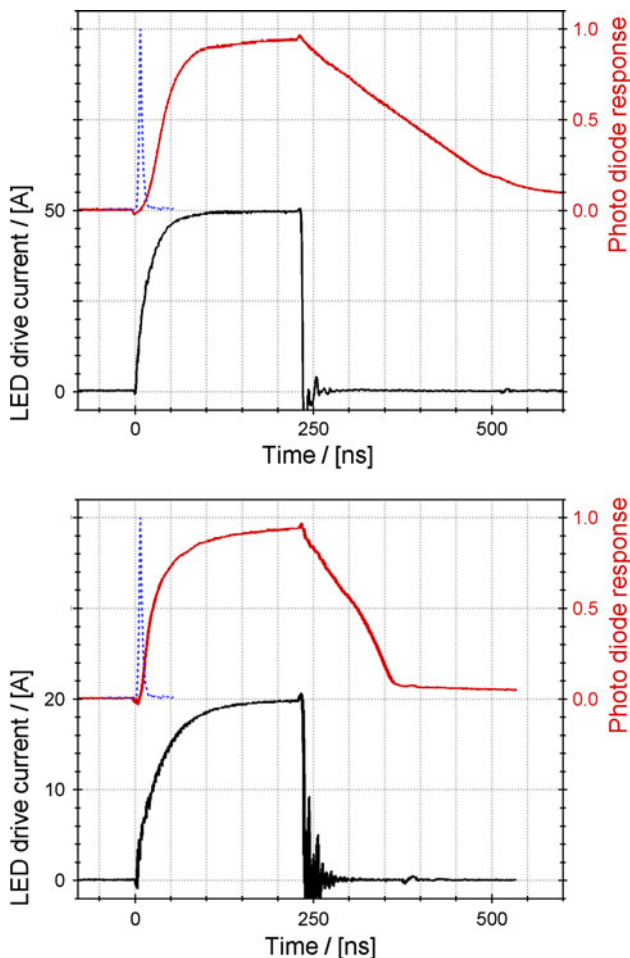


Fig. 2 Response of two LED types to a single current pulse of 250 ns duration as monitored by a photodiode: Luminus CBT-120-G (*top*) and Philips Luxeon LXHL-PM02, 5W (*bottom*). The *blue (dotted)* trace shows the photodiode response to a light pulse of an Nd:YAG laser

time seems to scale with device size: the larger Luminus device has a die size of $3 \times 4 \text{ mm}^2$ compared to about $2 \times 2 \text{ mm}^2$ of the smaller Philips Lumileds LED. At the same time, the smaller LED only has a fraction of the light emission (160 vs. 2,100 lm) and thus is considered unsuitable for the present high-speed schlieren imaging application. To demonstrate that the observed decay time is not an artifact, the same reverse-biased PIN photodiode (Thorlabs DET10A) was used to measure the pulse of an flashlamp pumped Nd:YAG laser with a specified pulse width of 5 ns. This signal is visible as a sharp spike at $t = 0$ in Fig. 2.

2.2 LED burst mode operation

The first application required a current pulse train of about 100 pulses, which were provided to the LED using a self-designed circuit similar to the circuit presented in (Willert

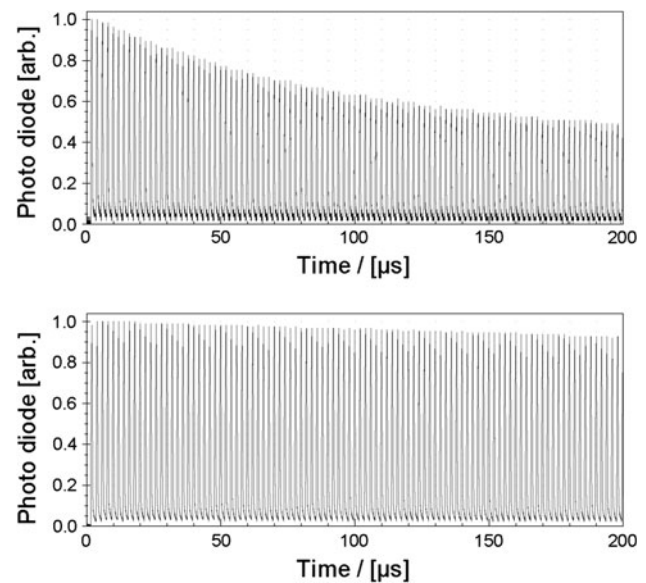


Fig. 3 Response of LED to a burst of 100 pulses (500 ns duration, 2 μs period) as monitored by a photodiode with different supply capacitances **C1**: 100 μF (*top*) and 2,200 μF (*bottom*)

et al. 2010). The commercial device (LDP-V 50-100 V3, PicoLAS GmbH) used initially was found not to have sufficient capacitance ($\approx 10 \mu\text{F}$) to support a steady burst of pulses with nearly constant intensity. Figure 3 shows the response of a fast, reverse-biased PIN photodiode (Thorlabs DET10A) to the pulsed light emission of the Luminus LED. By further increasing the supply capacitance **C1** from 100 to 2,200 μF , a train of pulses of nearly constant intensity could be achieved.

Figure 4 shows a portion in the middle of the 100 pulse train presented in Fig. 3 and demonstrates the pulse-to-pulse uniformity delivered by the LED. Each pulse has a width of 500 ns at a period of 2 μs (500 kHz). While the drive current has a rise time on the order of 100 ns, the LED responds much slower and does not reach a steady value before the end of the electrical pulse. The electroluminescence decay time is of similar order dropping to about 5 % of the maximum light emission in between the pulses.

The transient burst mode of operation allows the LED to be operated well beyond its design limits. In the presented application, the drive current reaches maximum values exceeding $I_f = 120 \text{ A}$. If summed over 100 pulses, the LED is effectively subjected to a 50 μs pulse of about $I_f = 120 \text{ A}$, which would result in immediate damage to the device, given the data presented in (Willert et al. 2010): At a pulse width of 50 μs , the maximum single pulse drive current was found to be about 65 A (The manufacturer quotes an absolute maximum current of 36A (Luminus 2008)). The reason the diode survives the current pulse train is the limited duty cycle (25 %) of the pulses allowing

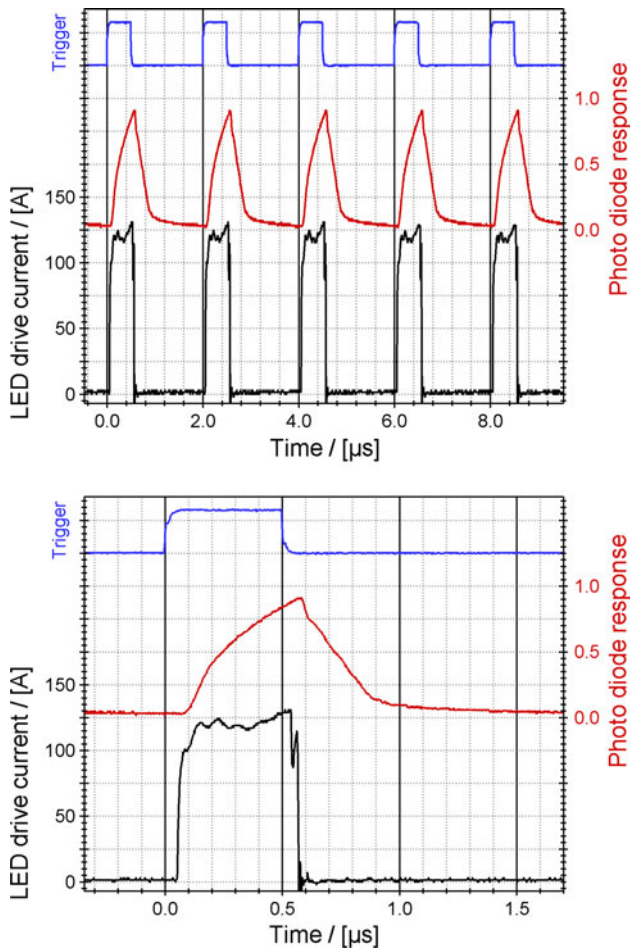


Fig. 4 Response of LED to a current pulse train as monitored by a photodiode, with lower plot showing detail of above. Legend: TTL trigger pulse (*top trace*), photo diode response (*middle trace*), LED drive current (*lower trace*)

the LED substrate (die) to cool in between the drive pulses. No systematic experiments have been performed to determine the maximum pulse currents for the limited (100) pulse train. The second application presented herein involved continuous pulsing of the LED at 1 kHz with drive currents exceeding $I_f = 120$ A at a much lower duty cycle (0.5 %), which does not introduce significant heat generation within the device.

Both a green and red LED of the Luminus Phlatlight CBT-120 series were tested for their suitability as light sources in the megahertz rate schlieren setup described in the following section. While the specifications (Luminus 2008) indicate that the red LED provides about one-third more radiometric flux (5.5W) than the green LED (4.1W), the former emits its light into a wider angular cone, that is, it has a higher divergence as shown in Fig. 5. As schlieren imaging configurations typically have a low numerical aperture, the additional light emitted by a given light source has no contribution. The data presented in Fig. 5 are

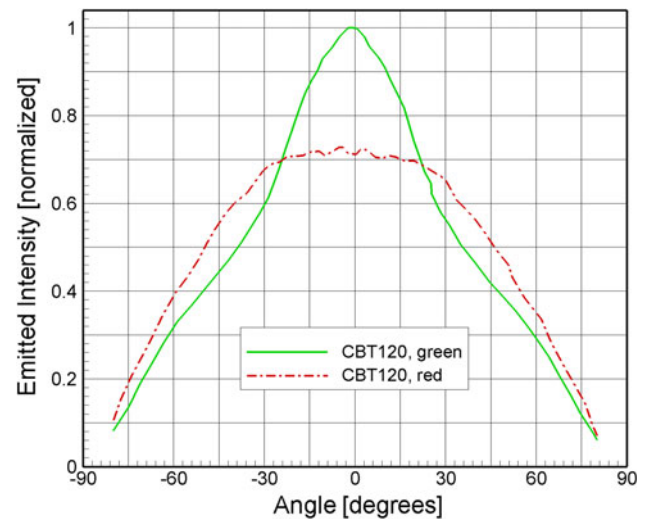


Fig. 5 Angular emission of Luminus Phlatlight (TM) LEDs (from Luminus 2008)

normalized with respect to each other and indicate that along the central axis, the red LED emits about 30 % less light in comparison to the green LED. From the radiometric point of view, both devices should, therefore, provide roughly the same amount of light within a low-aperture schlieren configuration. In practice, however, the green LED was found to provide brighter images and was selected for the schlieren imaging experiments. This difference is attributed to a higher sensitivity of the camera detector to green light.

The high current density in the LED causes the center wavelength of the electroluminescence to shift by about 20 nm from 530 nm to a cyan color (510 nm) at currents exceeding 100A (Willert et al. 2010). While the radiometric flux may be larger with increasing currents, this again has to be normalized against the wavelength-dependent sensitivity of the camera sensor to assess the actual improvement.

3 High-speed schlieren imaging of a supersonic jet

3.1 Burst mode schlieren image at up to 1 MHz

The pulsed LED light source described in the previous section was used to image the unsteady flow of an under-expanded free jet impinging onto a solid surface. This was achieved by synchronizing the LED driving electronics to a high-speed camera (Shimadzu HPV-1, 312×260 pixel (Etoh et al. 2002)). The LED (Luminus, Phlatlight CBT-120, green (Luminus 2008)) was pulsed in burst mode for 102 images at currents of up to 120 Ampere with 500 ns pulse duration.

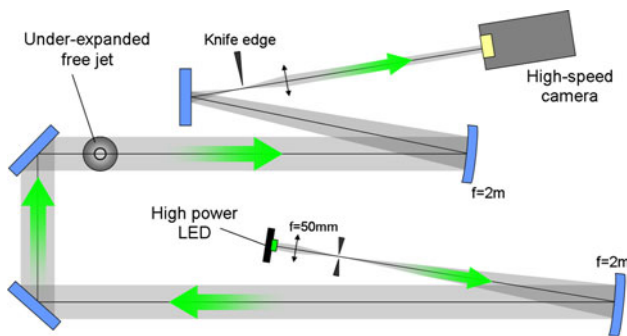


Fig. 6 Schlieren imaging setup with pulsed high-power LED as light source

A schematic of the schlieren imaging setup is shown in Fig. 6. Further details of the jet facility and the schlieren setup are described in (Risborg et al. 2008, Risborg 2008). The jet nozzle has a diameter of $D = 5$ mm. The stagnation pressure is measured by a transducer mounted in the plenum with a precision of ± 2 %

Figure 7 shows a subset of five successive schlieren images acquired with the LED as a light source. The high repeatability in illumination intensity allows the calculation of reliable statistics such as distributions mean intensity and corresponding standard deviation, shown in Figs. 8 and 9, respectively. These were calculated from ten image sequences of 100 frames acquired in short succession. The mean intensity data are then subtracted from the original sequences to highlight only the unsteady features in the images as shown in Fig. 10. Static features such as blemishes on the mirror surfaces are also reduced.

The schlieren flow visualization shows a jet at a nozzle pressure ratio (NPR) of 5.2, defined as the ratio of plenum stagnation pressure to ambient pressure. The impingement plate is positioned at a distance of $x = 15$ mm ($x/d = 3.0$). The jet core is characterized by the presence of a strong Mach disk, as well as an intermittent stand off shock above the plate (most evident in first and fourth images of the sequence). This combination of pressure ratio and impingement distance produces an oscillatory helical instability in the jet. The axial and radial position of the Mach disk is seen to vary from frame to frame, and a tilt about the x -axis is also evident, though somewhat more difficult to see in the still images. The size and shape of the standoff shock also fluctuates from image to image, not being evident at all in the final image.

The high temporal resolution of the camera combined with the short exposure time of the illumination system means that the evolution of individual acoustic waves can also be resolved in the flow visualization. In the present image set, there is a clear asymmetry in the acoustic field, which is almost certainly the result of the dominance of the

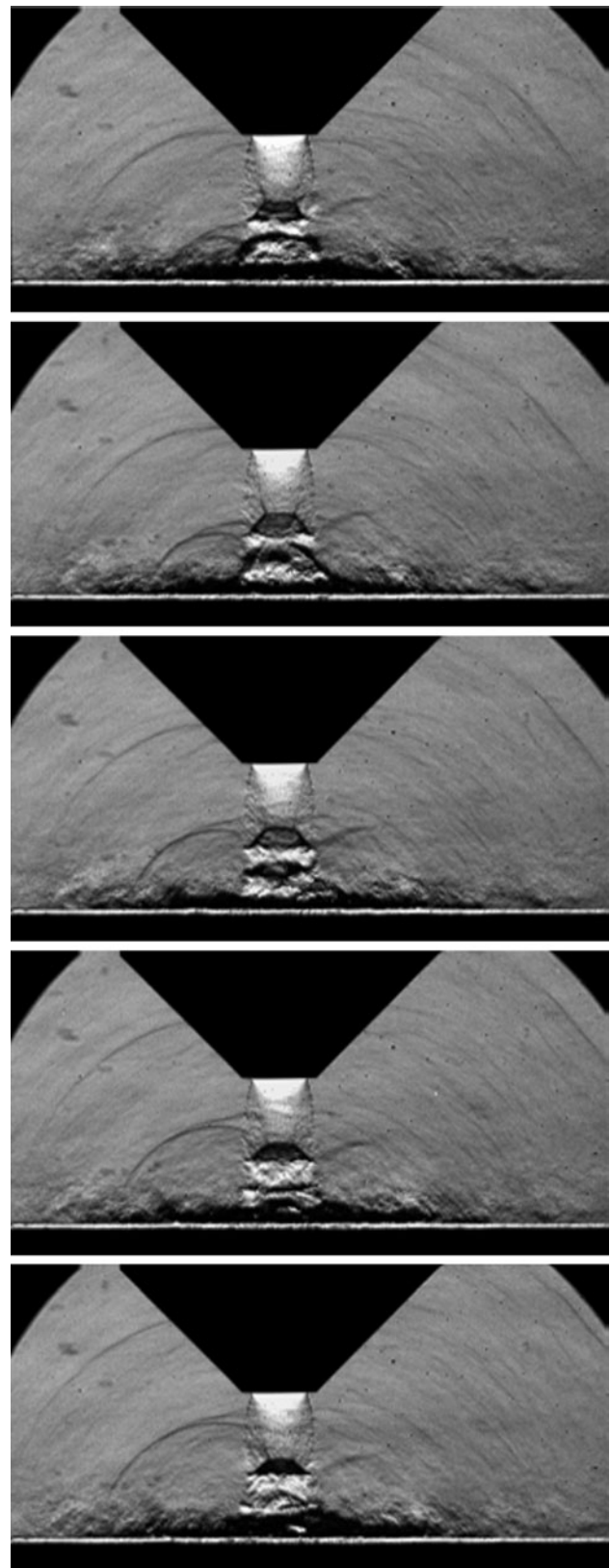


Fig. 7 Sequence of images spaced at $5 \mu\text{s}$ intervals obtained at nozzle pressure ratio 5.2, $x/D = 3.0$

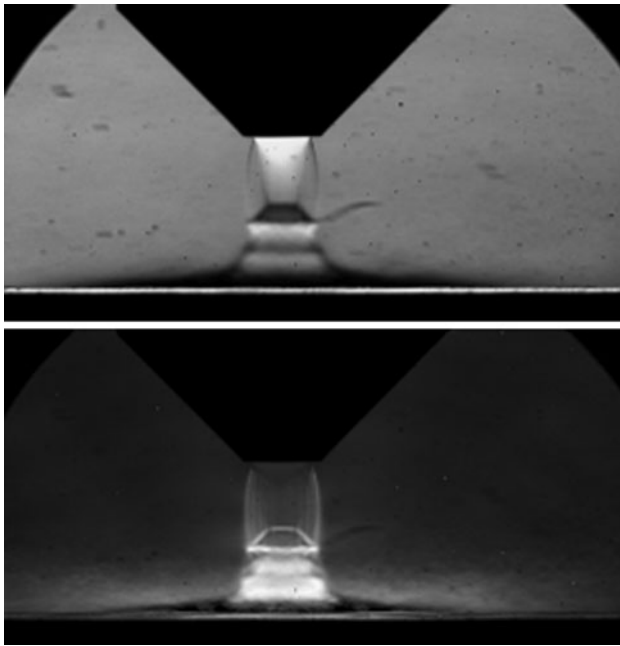


Fig. 8 Mean (*top*) and standard deviation intensity images (*below*) obtained from 10 sequences recorded in succession. Experiment parameters: nozzle pressure ratio 5.2, $x/D = 3.0$

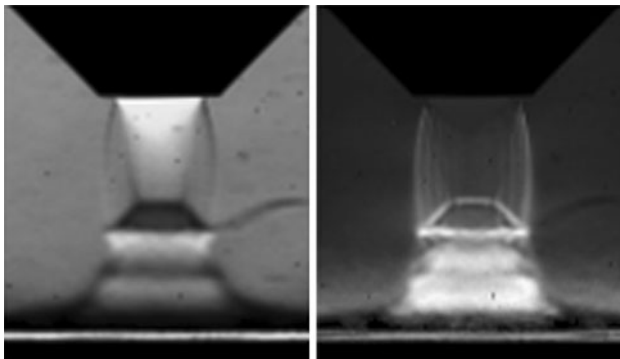


Fig. 9 Detail of Fig. 8, mean (*left*) and standard deviation (*right*)

helical instability in the jet. Previous work (Henderson 2003, 2005) has demonstrated that the production of sound waves is an outcome of fluctuations in the wall jet, driven by the arrival of coherent structures convected down the primary jet. As the impinging structures are helical, the resulting sound field will also be helical. Given that schlieren is a path-integrated technique, the resulting image shows a staggered sequence of acoustic waves appearing on either side of the primary jet.

In addition to the examples shown here, a fluid dynamics video showing selected sequences at four different nozzle pressure ratios are available for download from arXiv (Willert et al. 2010).

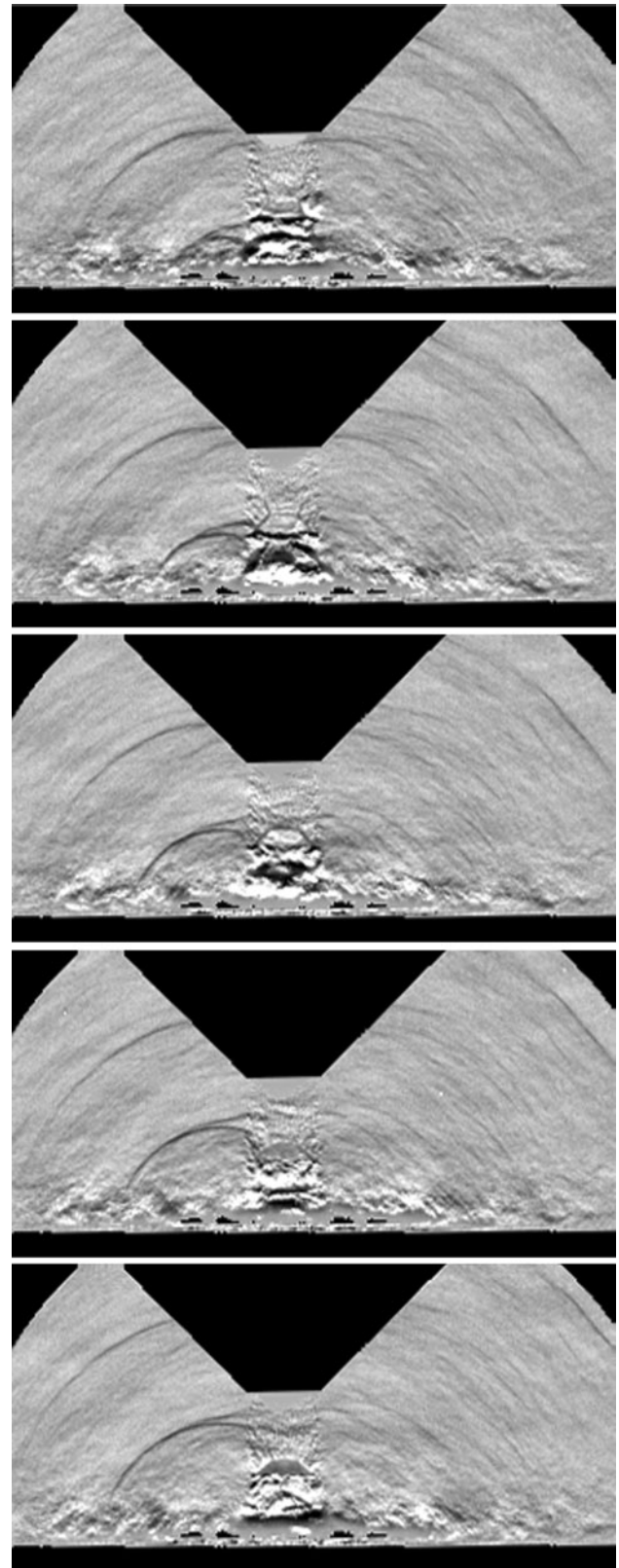


Fig. 10 Sequence of images spaced at 5 μs intervals obtained at nozzle pressure ratio 5.2, $x/D = 3.0$ (mean intensity shown in Fig. 8 subtracted)

3.2 Continuous pulsed schlieren imaging of a free jet

The pulsed LED sources also offer an alternative to stroboscopic sources for long-duration, moderate frame rate experiments. A second set of experiments is presented where the image acquisition was performed with a PCO Dimax camera ($2,016 \times 2,016$ pixel) operating at a frame rate of 1,000 frames per second. At this frame rate, the convection and evolution of individual structures cannot be observed; however, the system allows for the acquisition of images at significantly higher resolution and in large enough sample sizes to undertake statistical analysis.

To demonstrate the potential of the system, it is applied to a similar experimental facility to that described in the previous section, though the nozzle diameter is increased to 15 mm. It should also be noted that the compact dimensions of the LED's emitter ($3 \times 4 \text{ mm}^2$) already make it appropriate for a schlieren light source, as described in (Settles 2001). Therefore, no condenser lens and slit system was required, which further simplified the optical setup. A free jet operating at $\text{NPR} = 2.93$, where a strong screech tone exists, was the subject of the experiment.

With the LED pulsed for $2 \mu\text{s}$ at $I_f \approx 100 \text{ A}$ synchronous to the camera frame rate, a sequence of 6,300 images was obtained. Once again it should be emphasized that each image must be considered independent from its predecessor in the sequence. In this low duty cycle, continuous pulsing mode, the LED drive electronics operate in a steady-state manner, in which the pulse-to-pulse intensity

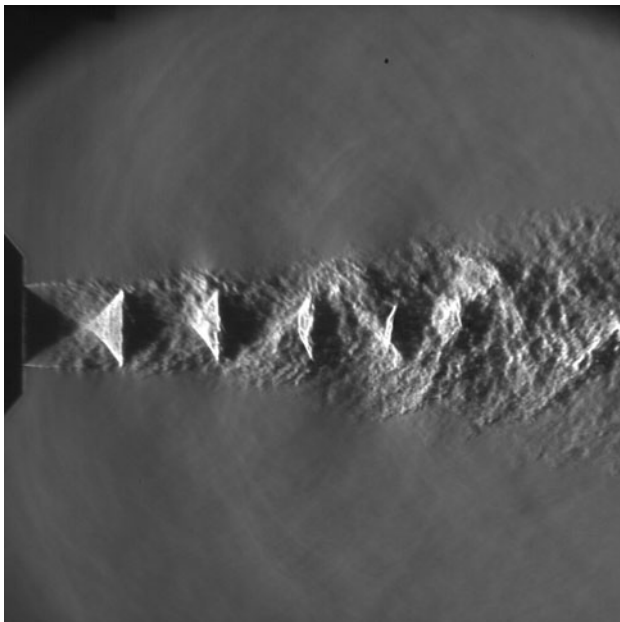


Fig. 11 Schlieren image of a free jet obtained at nozzle pressure ratio $\text{NPR} = 2.93$ and an effective pulse duration of $2 \mu\text{s}$

variations become insignificant, that is, there is no exponential intensity decay as shown in Fig. 3.

Figure 11 shows a representative instantaneous image from the sequence. The system setup visualizes the density gradient along the jet axis, $\frac{d\rho}{dx}$. The sinuous bright band evident from the third shock cell onwards is suggested to be evidence of the theorized helical vortex that is associated with certain screech tones, as described in (Umeda 2002). Both upstream and downstream traveling acoustic waves are also visible, though without the impingement plate to drive the feedback cycle, they are of much lower magnitude, and thus less distinct.

While the acoustic waves are visible in the single instantaneous images, they are far from clear, and little information about the acoustic field can be extracted by visual inspection. With the ability to produce large data sets quickly, a two-point correlation technique can be applied to extract further information from the flow. The two-point correlation is defined as follows:

$$R(\Delta x, \Delta r) = \frac{\sum I(x_0, r_0) \cdot I(x_0 + \Delta x, r_0 + \Delta r)}{\sum I(x_0, r_0)} \quad (1)$$

The correlation of the fixed point, (x_0, r_0) , with every other point in the image is calculated across the entire sequence. The quantity being correlated, the image intensity, does not correspond directly to any fluid property, but is rather a representation of the path integral of the refractive index through the depth of the flow field. Nonetheless, it is useful to investigate the macroscopic properties of the flow, in particular the interaction between the jet and the acoustic field.

A sample correlation map is displayed in Fig. 12. The fixed point, (x_0, r_0) , is indicated by the intersection of the overlaid dotted lines. The correlation is obviously much stronger in the jet core than in the surrounding acoustic

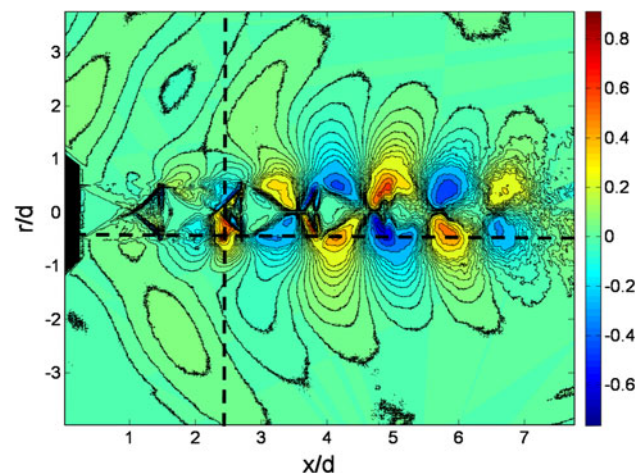


Fig. 12 Two-point correlation data of a free jet obtained at nozzle pressure ratio $\text{NPR} = 2.93$

field, so the contour levels have been adjusted so that both are visible. The influence of the helical instability is immediately apparent in the alternating cells of high and low correlation on either side of the jet centerline. At each axial point, the correlation above and below the centreline is of opposite sign. This extends also into the acoustic field, with the helical nature of both the upstream and downstream traveling acoustic waves evident in the correlation map.

Comparison of Figs. 11 and 12 shows that the statistical analysis of large data sets can yield valuable information even from relatively qualitative visualizations such as schlieren image sequences. The use of the pulsed LED system allows for fine control of both acquisition rate and exposure time, independent of the camera system used.

4 Discussion and summarizing remarks

As mentioned in the previous section, one of the advantages of the LED system is that the LED itself intrinsically possesses a geometry that makes it appropriate for use as a Schlieren light source. Settles (2001) states “a rectangular light source with overall dimensions of a few mm is most suitable for schlieren imaging according to sensitivity and measuring-range considerations”. While it may in some cases still be desirable to use a condenser-slit system, it is no longer necessary to do so with an LED light source. This reduces the number of components needed and space required for the schlieren system. With regard to LED selection, both the angular emission profile and wavelength also influence the performance in a schlieren imaging setup; in the present application, a green LED was found to outperform a seemingly brighter red LED.

The pulsed LED system also offers a significant advantage in ease of alignment compared to many other pulsed light sources. The LED can be operated in its “normal” continuous mode, or pulsed quickly enough to appear continuous to the human eye. This greatly simplifies the alignment and setup process, as the focus and schlieren cutoff can be adjusted in real time. Both the low operating voltage of the LED as well as the non-collimated nature of the emitted light reduce operational hazards. Even though the LEDs were operated well beyond their specifications, no devices were damaged during the experiments. The actual safe operating limits for LEDs operated in burst mode so far have not been investigated by the authors.

While the attentive reader may rightfully observe that a high-speed camera can be shuttered to reduce motion blur instead of pulsing the LED, it should be observed that the LED will not survive a continuous pulse for the duration of the image sequence acquisition (120A for 100 μ s). The real advantage of the pulsed LED operation manifests itself as

soon as the pulsing frequencies are reduced to values in the 100 kHz range and below. Recording longer image sequences at these frequencies requires pulse durations in the millisecond range and longer, which is beyond the flash duration of conventional xenon flash lamps and would require high brightness continuous light sources. For example, in order to match the intensity of the 2 μ s LED pulses at 1 kHz frame rate as presented in Sect. 3.2 would require a continuous light source with a 500 times higher average intensity.

Although not an issue in mirror-based schlieren setups, the narrow bandwidth of the LED electroluminescence (about 35 nm FWHM for green LEDs) improves image contrast in comparison to white light illumination due to the reduction of chromatic aberration effects in the optical setup. While the highly coherent light provided by laser sources makes a conventional schlieren system very susceptible to diffraction effects at the knife edge and introduces speckle effects on the sensor, these issues are effectively avoided by the short coherence length of the LED.

The high repeatability of the LED pulse trains makes the acquired data suitable for statistics-based imaging involving a multitude of image sequences. This is exemplified by the two-point correlation data shown in Fig. 12.

A key advantage of the LED is that with a single illumination system, a range of different image acquisition parameters may be covered. The pulse rate, pulse width, brightness, and acquisition duration are all independent parameters, allowing for a significant flexibility in the system. All parameters may be varied arbitrarily during the experiment, allowing the user complete control over all aspects of the illumination. For instance, the essentially lag-free light emission of an LED in response to an external trigger event allows the system to capture phase steady image data of cyclic recurring events of continuously varying frequency.

Beyond the high-speed schlieren imaging applications presented herein, pulsed LED illumination has been demonstrated both for flow field measurement, in particular particle image velocimetry (PIV) (Stasicki et al. 2010; Willert et al. 2010), as well as for high speed droplet shadow imaging of spray systems (Klinner 2011; Willert et al. 2008, 2010).

Acknowledgments The financial support of this research by the Australian Research Council is gratefully acknowledged.

References

- Bretthauer B, Meier GEA, Stasicki B (1991) An electronic Cranz–Schardin camera. *Rev Sci Instrum* 62(7):364–368. doi: [10.1063/1.1142129](https://doi.org/10.1063/1.1142129)
- Buttsworth DR, Sercombe DBT (2008) Cranz–Schardin visualisation of a hypersonic cone with gas injection. In: 28th International

- congress on high-speed imaging and photonics, SPIE vol 7126. University of New South Wales at ADFA, Canberra. doi:[10.1117/12.822032](https://doi.org/10.1117/12.822032)
- Deblock Y, Ducloux O, Derbesse L, Merlen A, Pernod P (2007) High speed single charge coupled device Cranz–Schardin camera. *Rev Sci Instrum* 78(3):035,111–1–035,111–4. doi:[10.1063/1.2714771](https://doi.org/10.1063/1.2714771)
- Etoh TG, Poggemann D, Ruckelshausen A, Theuwissen A, Kreider G, Folkerts HO, Mutoh H, Kondo Y, Maruno H, Takubo K, Soya H, Takehara K, Okinaka T, Takano Y, Reisinger T, Lohmann C (2002) A ccd image sensor of 1 mframes/s for continuous image capturing of 103 frames. In: IEEE International solid-state circuits conference, 2002, digest of technical papers. ISSCC, vol 1, pp 46–443. San Francisco, CA, USA. doi:[10.1109/ISSCC.2002.992931](https://doi.org/10.1109/ISSCC.2002.992931)
- Henderson B (2003) The connection between sound production and jet structure of the supersonic impinging jet. *J Acoust Soc Am* 111(n2):735–774. doi:[10.1121/1.1436069](https://doi.org/10.1121/1.1436069)
- Henderson B, Bridges J, Wernet M (2005) An experimental study of the oscillatory flow structure of tone-producing supersonic impinging jets. *J Fluid Mech* 542:115–137. doi:[10.1017/S0022112005006385](https://doi.org/10.1017/S0022112005006385)
- Hiller W, Lent HM, Meier GEA, Stasicki B (1987) A pulsed light generator for high speed photography. *Exp Fluids* 5(2):141–144. doi:[10.1007/BF00776185](https://doi.org/10.1007/BF00776185)
- Klinner J, Willert C (2011) On the implementation of tomographic shadowgraphy for spray diagnostics. In: 9th International symposium of particle image velocimetry (PIV'11). Kobe University, Kobe, Japan
- Luminus Devices, Inc (2008) Technical product data sheet PDS-001226: CBT-120 series, PhlatLight LED Illumination products
- Risborg A, Mitchell D, Honnery D, Soria J (2008) Instabilities in underexpanded impinging jets. In: Fifth Australian conference on laser diagnostics in fluid mechanics and combustion. The University of Western Australia
- Risborg A, Soria J (2008) High-speed optical measurements of an underexpanded supersonic jet impinging on an inclined plate. In: 28th International congress on high-speed imaging and photonics, SPIE vol 7126. UNSW at ADFA, Canberra. doi:[10.1117/12.822137](https://doi.org/10.1117/12.822137)
- Settles GS (2001) *Schlieren and shadowgraph techniques*. Springer, Berlin
- Stasicki B, Hiller W, Meier GEA (1984) Hochfrequenz-Stroboskop mit LED-Lichtquelle. *Tech Messen* 51:217–220
- Stasicki B, Hiller W, Meier GEA (1990) Light pulse generator for high speed photography using semiconductor devices as a light source. *Opt Eng* 29(7):821–827. doi:[10.1117/12.55647](https://doi.org/10.1117/12.55647)
- Stasicki B, Kompensans J, Willert C (2010) Pulsed high-power LED illuminator for the visualisation and measurement of flows. In: ISFV14—14th International symposium on flow visualization, ISFV14-3E-6 206, pp 1–8. <http://elib.dlr.de/62801/>
- Umeda Y, Ishii R (2002) Existence of mach cones and helical vortical structures around the underexpanded circular jet in the helical oscillation mode. *J Acoust Soc Am* 112:99–107. doi:[10.1121/1.1487839](https://doi.org/10.1121/1.1487839)
- Willert C, Freitag S, Hassa C (2008) High speed imaging of fuel sprays using a low-cost illumination source. In: 22nd European conference on liquid atomization and spray systems (ILASS 2008). <http://elib-v3.dlr.de/55164/>
- Willert C, Mitchell D, Soria J (2010) Megahertz schlieren imaging of shock structure and sound waves in under-expanded, impinging jets. *arXiv physics.flu-dyn*. <http://arxiv.org/abs/1010.3186v1>
- Willert C, Moessner S, Freitag S, Hassa C (2010) High speed shadowgraphy of a combusting air blast atomizer spray at elevated pressure. In: 23rd Annual conference on liquid atomization and sprays, ILASS Europe 2010. <http://elib.dlr.de/65220/>
- Willert C, Stasicki B, Klinner J, Moessner S (2010) Pulsed operation of high-power light emitting diodes for imaging flow velocimetry. *Meas Sci Technol* 21(7):075,402. <http://stacks.iop.org/0957-0233/21/i=7/a=075402>